Retrieving Winds in the Surface Layer over Land Using an Airborne Doppler Lidar

K. S. GODWIN

Department of Environmental Sciences, University of Virginia, and Simpson Weather Associates, Inc., Charlottesville, Virginia

S. F. J. DE WEKKER

Department of Environmental Sciences, University of Virginia, Charlottesville, Virginia

G. D. EMMITT

Simpson Weather Associates, Inc., Charlottesville, Virginia

(Manuscript received 16 August 2011, in final form 22 December 2011)

ABSTRACT

Airborne Doppler wind lidars are increasingly being used to measure winds in the lower atmosphere at higher spatial resolution than ever before. However, wind retrieval in the range gates closest to the earth's surface remains problematic. When a laser beam from a nadir-pointing airborne Doppler wind lidar intercepts the ground, the return signal from the ground mixes with the windblown aerosol signal. As a result, winds in a layer adjacent to the surface are often unreliable and removed from wind profiles. This paper describes the problem in detail and discusses a two-step approach to improve near-surface wind retrievals. The two-step approach involves removing high-intensity ground returns and identifying and tracking aerosol radial velocities in the layer affected by ground interference. Using this approach, it is shown that additional range gates closer to the surface can be obtained, thereby further enhancing the potential of airborne Doppler lidar in atmospheric applications. The benefits of the two-step approach are demonstrated using measurements acquired over the Salinas Valley in central California. The additional range gates reveal details of the wind field that were previously not quantified with the original approach, such as a pronounced near-surface wind speed maximum.

1. Introduction

Doppler lidars have the ability to accurately retrieve atmospheric winds at high spatial and temporal resolution. Because of the reduction in cost, size, and power consumption of lasers, Doppler wind lidars are becoming more accessible to the atmospheric research community (Werner 2005) and their use has become more widespread. Many important insights into atmospheric flow patterns have been obtained from ground-based (e.g., Post and Neff 1986; Banta et al. 1993; Drobinski et al. 2003; Banta et al. 2004; Rucker et al. 2008) and airborne (Reitebuch et al. 2003; Weissmann et al. 2005; Bastin et al. 2005, 2006; De Wekker et al. 2012, hereafter DEW) Doppler lidars. Compared to ground-based lidars, airborne lidars have larger spatial coverage but are more expensive to operate, require platform motion compensation, and have been used less frequently. In the United States, airborne Doppler lidar flights have mostly been performed in the California Monterey Bay area with a Naval Twin Otter aircraft (Emmitt et al. 2005). These flights were originally motivated by the need to develop and improve data-processing techniques to analyze data from the potential future installation of Doppler lidars on space-based platforms (Menzies 1986; Baker et al. 1995). Meanwhile, it has been well established that the assimilation of airborne and spaceborne Doppler lidar data in numerical weather prediction models can improve weather forecasts (Weissmann and Cardinali 2007; Pu et al. 2010). Therefore, it is expected that use of airborne Doppler lidars in research of atmospheric dynamics and weather forecasting will increase in the near future, making the further development of lidar data-processing techniques desirable. The purpose of this paper is to contribute to

Corresponding author address: Stephan F. J. De Wekker, P.O. Box 400123, 291 McCormick Rd., Department of Environmental Sciences, University of Virginia, Charlottesville, VA 22904-4123.
E-mail: dewekker@virginia.edu

DOI: 10.1175/JTECH-D-11-00139.1

TABLE 1. Characteristics of the Twin Otter Doppler lidar system. Radial velocity accuracy is optimum and based on hard target returns.

Wavelength	2 μm (eye safe)
Energy per pulse	2 mJ
Pulse repetition frequency	500 Hz
Range resolution	50 m
Radial velocity measurement accuracy	0.05 m s^{-1} per single shot with ground calibration
Wind component accuracy (assuming homogeneous flows with 12 pt. VAD processing)	u, v, w 0.1 m s^{-1}
Pulse length (full width half maximum)	90 m

this development by improving the retrieval of winds near the surface, which is difficult because of ground interference. After providing some background information about the airborne Doppler lidar and summarizing some important steps in the data-processing techniques in section 2, we will describe the effect of ground interference on airborne Doppler wind retrieval in section 3. The approach to address the issue is discussed in section 4, followed by a demonstration of the improvements in the near-surface wind retrieval in section 5. We discuss the limitations of the approach and possible alternative approaches in section 6, and conclude with a summary in section 7.

2. Lidar data

We use data from a 2-μm coherent Doppler lidar mounted on a Navy Twin Otter aircraft [the Twin Otter Doppler wind lidar (TODWL)]. Table 1 gives some technical details of TODWL. A discussion of the accuracy and precision of TODWL is provided in DEW. TODWL utilizes a biaxis scanner mounted on the side of the aircraft allowing it to scan the atmosphere above, below, or in front of the aircraft. Data used in this study were obtained using a downward-looking conical scanning pattern while the aircraft was flying over the Salinas Valley and its adjacent mountains on 12 November 2007. DEW describe the wind and aerosol structure on this day, which was characterized by the presence of thermally driven flows in the Salinas Valley. TODWL flew at a height of 3000 m mean sea level (MSL) at a ground speed of between 50 and 60 m s^{-1}.

The raw lidar data consist of the transmitted signal and the windblown aerosol backscattered (or return) signal. The backscattered signal is mixed on the detector with the signal from a local oscillator. The local oscillator's frequency has been offset to allow the use of a simple ''real'' fast Fourier transform (FFT) to detect both positive and negative frequency shifts from the zero velocity reference frequency. An analog front end used with the TODWL continually adjusts the zero frequency to remove the component of the aircraft velocity projected onto the line of sight and to account for changes in scanner angles (both azimuth and elevation). The return signal's intensity can span several orders of magnitude because of the wide range of aerosol backscatter intensities, as well as the range-squared effects. Thus, the raw signal passes through log amplification, which compresses the broad range of signal intensity for accommodation by an 8-bit digitizer providing 256 levels of resolution. Subsequent interpretations of the signal intensities are expressed in units of decibels (10 $\log_{10}$ signal). The signal-to-noise ratio (SNR) can be defined as the ratio of the signal intensity and the noise floor. The noise floor is calculated by processing the tail end of the signal that temporally would reside below the ground and averaging the spectrum.

Two major steps in the processing of Doppler lidar data involve 1) processing raw lidar data to produce radial velocities and 2) combining those radial velocities to produce three-dimensional winds. Most relevant for addressing the difficulty of retrieving near-surface winds from airborne Doppler lidar is the first step, as discussed next.

In the first major data-processing step, the spectral peaks in the frequency domain of the transmitted and return signals are determined by processing the signal data using an FFT. The Doppler shift between the peaks in the transmitted and the return signal is proportional to the radial velocity. A shift of 1 MHz in the peak frequency between the transmitted and backscattered signal corresponds to a velocity of 1 m s^{-1} for the 2-μm TODWL. The frequency of each transmitted pulse is monitored and used to correct the derived radial velocity for laser frequency jitter. The first data-processing step involves many details, including correcting for aircraft attitude and determining the number of vertical range gates. Early challenges to the determination of radial velocities from airborne Doppler lidar include inaccurate measurements of the position and attitude of the aircraft and the retrieval of radial velocities in a weak and noisy backscattered aerosol signal resulting from attenuation or to a small numbers of aerosols in the atmosphere. Efforts to increase the signal strength have focused on accumulating the spectra for multiple laser pulses along a single line of sight (Rye and Hardesty 1993a,b; Smalikho 2003). Accumulating laser shots or spectra is made possible by high pulse repetition systems, and also by implementing a scanning pattern in which multiple laser pulses are transmitted at a particular azimuth angle for a certain time. Such a step–stare conical scanning pattern is used by TODWL where, for each azimuth angle or line of sight, ~500 lidar pulses are transmitted into the atmosphere of which 166 backscattered pulses are digitized at 100 MHz. Only 166 of the 500 pulses are recorded because of hardware limitations. Each line of sight contains all range ''gated'' radial velocities for a particular azimuth angle. The range resolution of the wind profile is limited by the full width at half maximum (FWHM) of the lidar pulse, which is approximately 90 m. By overlapping/sliding the raw signal data by about 50% our wind profiles provide range gates every 50 m. Thus, there is weak correlation between adjacent range gates. In this processing step, each radial velocity estimate is also corrected for platform motion and attitude. These corrections are made based upon data from a global positioning system (GPS)/inertial navigation system (INS), which is located in close proximity to the lidar to avoid errors resulting from data system time delays and aircraft flexures.

In the second major data-processing step, the wind vector is derived from radial velocities using the well-known velocity–azimuth display (VAD) technique (Lhermitte and Atlas 1961; Browning and Wexler 1968). This method was originally developed for continuously scanning ground-based radars looking up into the atmosphere. In this technique, the wind vector is determined from radial velocities during an azimuthal scan. To derive the three-dimensional wind, a sine fit is applied to the radial velocities as a function of azimuth angle. To solve for the u, v, and w components of the wind, at least three radial velocities at different azimuth angles need to be measured (nadir angle is usually fixed). For the TODWL operations, typically 12 azimuth angles are used in a step–stare conical scanning pattern. The lidar is rotated through 30° azimuth intervals, with 1-s dwells (''stares'') and 1-s transition times (''steps'') resulting in a total of 12 radial velocities at each range gate in a full scan. A complete step–stare conical scan therefore takes about 24 s at an aircraft speed of 50–60 m s^{-1}, resulting in a wind profile obtained every 1200–1440 m. Because of these characteristics of the aircraft's slow speed and the lidar's rapid scanning, the vertical and horizontal resolution of derived three-dimensional wind profiles is higher than in previous studies using airborne Doppler lidars (e.g., Rahm 1995; Reitebuch et al. 2003; Weissmann et al. 2005) and makes the TODWL operations ideal for the investigation of local and mesoscale flow phenomena (DEW).

In the next sections, we describe the effect of ground interference on radial velocities using simulated and real examples and discuss and evaluate an approach to minimize this effect. For the real examples, we use the TODWL data.

3. The effect of ground interference on radial velocities

Airborne DWL radial velocities of the aerosol motion near the earth's surface can be difficult to identify because of the confounding nature of the reflected energy as the lidar pulse intercepts the ground. The reflectance of hard targets, such as the earth's surface, is substantially larger than the backscattered signal from aerosol particles. While the resulting maximum SNR is useful in identifying the location of the ground, the ground return also interferes with and overwhelms the desired aerosol signal just above the surface. The TODWL 2-μm Doppler lidar emits an electromagnetic pulse of energy that is essentially Gaussian shaped in intensity. Over the duration of the pulse, the frequency changes linearly from higher to lower frequencies in response to thermally induced laser cavity changes. This predictable frequency change is referred to as ''chirp.'' The amount of chirp in a pulsed lidar system varies depending upon the laser material and energy density. For the TODWL system, the chirp is characterized by a velocity equivalent sweep from approximately -2 to $+2$ m s^{-1} during the pulse. In a diffuse illuminated volume absent of clouds or regions of extremely high aerosol concentrations (e.g., smoke), the effects of the dynamic frequency within the pulse length do not affect the accurate retrieval of aerosol radial velocities. However, when the pulse is reflected from a hard target, the frequency chirp can be detected in the backscattered signal. It is this chirp signature that is particularly evident in ground returns and interferes with the accurate retrieval of aerosol radial velocities. The sequence of events as the pulse intercepts the surface is shown schematically in Figs. 1a–c. Note that as the pulse approaches the ground, the Gaussian-shaped intensity of the pulse is reflected from the ground much as it would be from a mirror. In this example when the center of the pulse is located at 200 m AGL, the leading edge of the pulse energy is being reflected from the ground (Fig. 1a) and will mix with the aerosol return reported for that same altitude. Therefore, at the 200-m AGL range gate the ground is reflecting the part of the pulse that is smaller in intensity than its maximum intensity. This ''early'' ground return results in a spectral peak (''ground peak'') that is consistent with a frequency shift corresponding to a radial velocity of -2 m s^{-1} for TODWL. Note that in this and other periodograms presented in this paper, we have converted frequency to radial velocity so that we can simply refer to the frequency peaks as radial velocities. The frequency of the transmitted signal is treated as 0 m s^{-1}, while the radial velocity related to the aerosol signal is, of course,

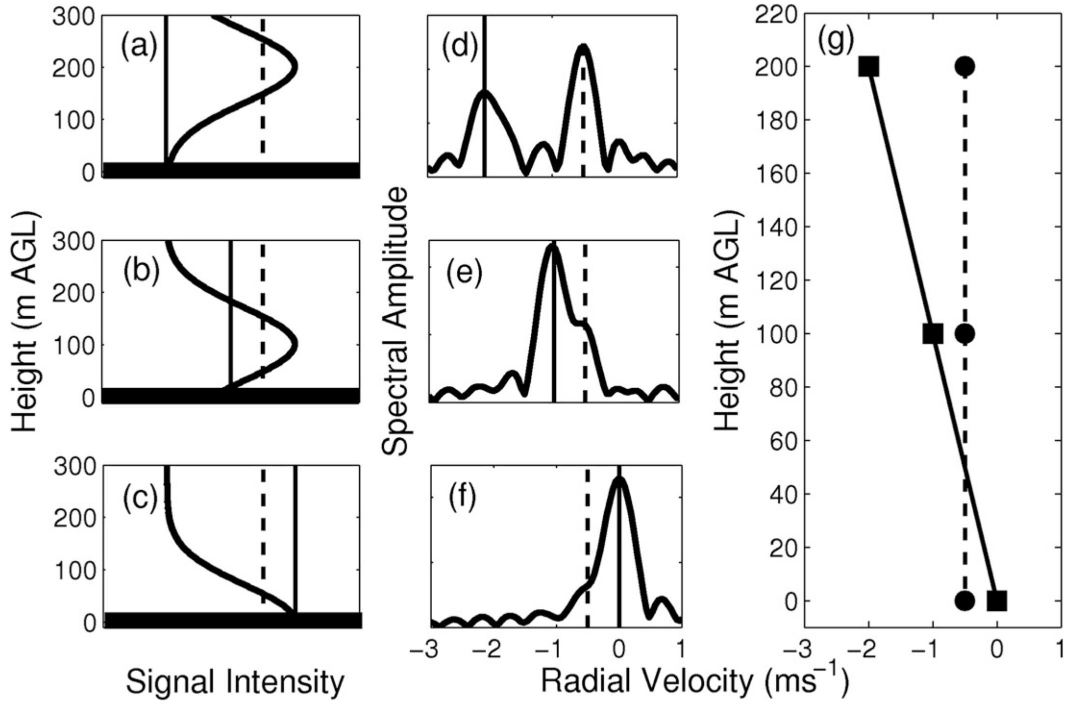

FIG. 1. A schematic of (a)–(c) the variation with height of the intensity of a Gaussian-shaped pulse as it approaches the surface, (d)–(f) the corresponding periodograms that indicate the radial velocities associated with the ground return (solid line) and the aerosol return (vertical dashed line), and (g) the corresponding radial velocity profiles. The radial velocity associated with the aerosol return [dashed line at -0.5 m s^{-1} in (d)–(g)] remains constant while the radial velocity associated with ground return (solid line) linearly shifts from -2 to 0 m s^{-1} at the ground. See text for explanation.

variable, and in the example of Fig. 1 equals -0.5 m s^{-1}. As the center of the pulse continues toward the ground (e.g., at 100 m), a different part of the pulse is reflected by the ground resulting in a shift of the ground peak to -1.3 m s^{-1} (Fig. 1b). Finally, when the center of the pulse intercepts the ground, the ground peak is at 0 m s^{-1} (Fig. 1c). Figures 1d–f shows this sequence of events. When the leading edge of the pulse is reflected from the ground, the ground return and the aerosol return overlap but are easily discernible from one another (Fig. 1d). At 100 m, the ground peak dominates (originating from 0 m) and overlaps the aerosol peak (at 100 m), making the aerosol peak harder to discern (Fig. 1e). Finally, as the pulse center reaches the ground, the aerosol peak becomes even less discernible (Fig. 1f). The characteristics and consistency of the ground's reflection of the laser's chirp signature facilitate a differentiation between the aerosol and the ground peak (this will be discussed in more detail in section 4b). The frequency shift from the leading edge of the TODWL's Gaussian pulse creates an identifiable linear radial velocity structure from about -2 m s^{-1} at a height between 100 and 300 m above the ground to 0 m s^{-1} at the ground, which is displayed in Fig. 1g.

We demonstrate ground interference with an example from real data in Fig. 2. The figure shows the spectral output for three different azimuth angles (columns) and three consecutive range gates (rows) from 200 to 100 m AGL after performing an FFT on the raw backscatter data. Multiple spectral peaks are discernible, and we are interested here in the primary (largest) peak and the secondary (second largest) peak. The ground and aerosol peaks switch from being the primary or secondary peaks. The data-processing routine selects the primary peak as the radial velocity. For the data in the 200-m range gate the primary peak is well defined and is correctly designated as the aerosol peak. A secondary peak is also typically present, but is smaller and distinguishable from the primary peak. This secondary peak is the ground peak and its presence indicates that some interference with the ground is occurring. In the range gate at 150 m (Figs. 2b,e,h), the ground peak has become stronger than the aerosol peak yet the aerosol peak is still resolvable. Eventually, the ground overwhelms the aerosol peak in the range gate at 100 m (Figs. 2c,f,i).

4. An approach to improve wind retrieval near the ground

To reduce the effect of ground interference and improve near-ground wind retrievals, we have experimented

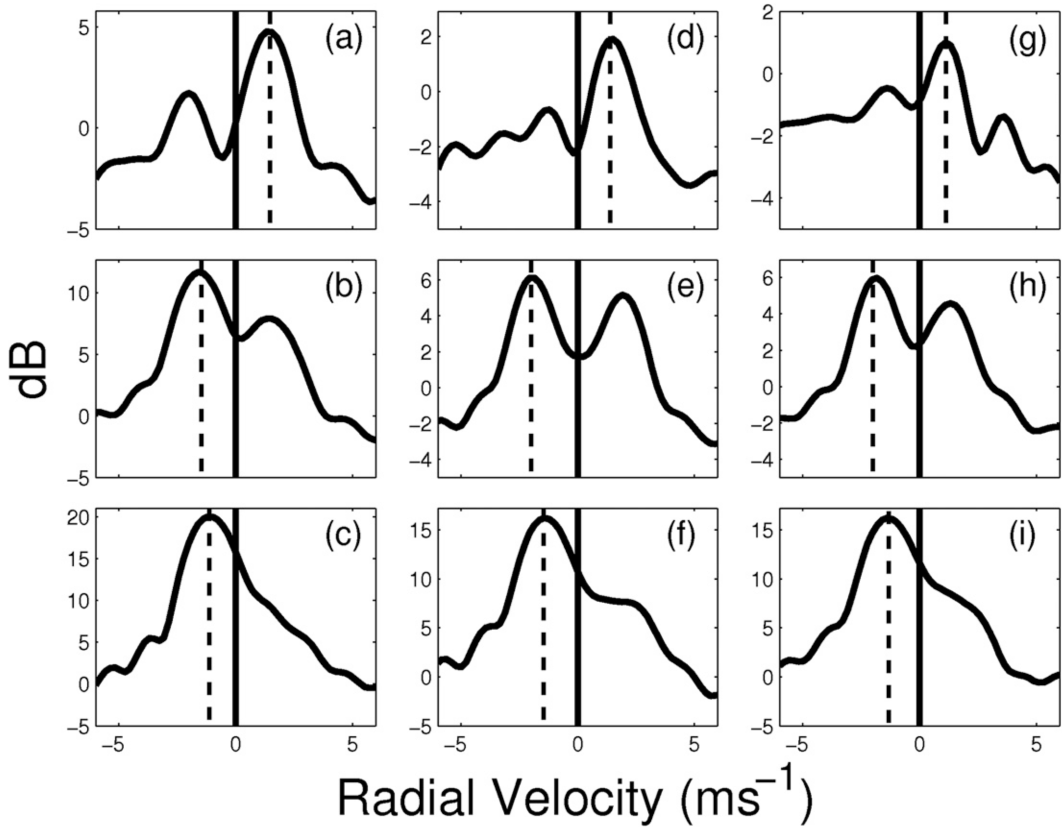

FIG. 2. Spectral output from applying FFT to the raw data for three different azimuth angles separated by 30° (columns) and three different range gates separated by 50 m (rows). Zero velocity as determined by transmitted/monitor pulse (solid vertical line) is denoted, as is the radial velocity associated with the primary peak (vertical dashed line).

with a two-step approach that includes 1) a method that reduces the amplitude of the ground peak (‘‘clipping''), and 2) a method that improves the identification and tracking of the aerosol peak (‘‘threading'').

a. Clipping

Our current approach to minimize the intensity of the ground backscatter signal is to apply a clipping filter. Clipping is a well-established method used to reduce nonrandom spectral peaks by first identifying what signal needs to be removed and then limiting its intensity prior to determining its spectral components (Van Vleck and Middleton 1966). Clipping essentially reduces the peak-to-average power ratio in a signal by clipping data that fall outside of a predetermined range. Our goal is to reduce the intensity of the ground return in the layers closest to the surface. We accomplish this by clipping the raw backscatter return in the time domain to reduce the spectral amplitude of the ground return in the frequency domain. The intensity of the backscattered pulse ranges from 1 to 256 dB through digitization. The clipping routine consists of various steps. The first step is to calculate the mean intensity of the raw return signal between 400 and 500 m above the ground. Next, all points within 400 m of the ground that fall outside of a predetermined range of 50 dB from the mean intensity are clipped and set equal to the mean. The value of 50 dB is a system-dependent value that should be determined by evaluating the aerosol signal intensity in a clear air environment over numerous shots. This value allowed for the retention of 98% of the signal, which represents a compromise between minimizing the effect on the aerosol signal (whose intensity is largely below 50 dB) while sufficiently reducing the ground return signal (at intensities larger than 50 dB). Sensitivity tests were done using 30- and 100-dB ranges. A 30-dB range (retaining 82% of the signal) made the aerosol peaks too small to be identified while a range of 100 dB (retaining almost 100% of the signal) had little effect on the suppression of the ground signal. A starting point of 400 m above the surface is used because the ground return typically starts interfering with the aerosol return in this region. Not all ground-generated data points fall outside the range of 50 mV from the mean intensity so

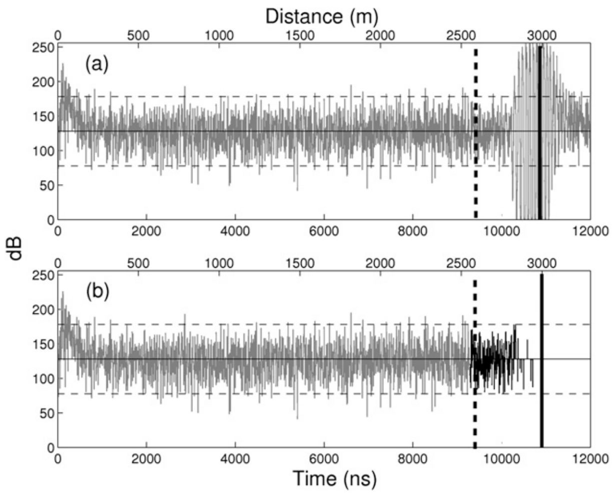

FIG. 3. Intensity of the backscatter signal as a function of distance from the lidar (or travel time) along the line-of-sight (a) before and (b) after applying the clipping routine. (top) Distance and (bottom) time are denoted. The ground (solid vertical line) and 400 m above the ground (dashed vertical line) are shown. The mean intensity between 400 and 500 m above the ground (solid horizontal line) and the allowed intensity range (dashed horizontal line) are also shown.

that ground interference is not completely eliminated. This procedure therefore minimizes the intensity of the ground peak while retaining necessary aerosol information. Figure 3 shows an example of applying the clipping routine to the backscattered lidar pulse. The intensity of the backscattered signal ranges from 1 to 256 dB and is plotted against time, which is converted to distance using the speed of light. A ground-generated region of high intensity is present at a distance between 2500 and 3000 m from the origin of the lidar pulse. Pure noise exists beyond the ground return and is not processed.

The ability to better discern the aerosol peak when the clipping routine is applied to the raw data is demonstrated in Fig. 4, which shows the spectral output for the same range gates as in Fig. 2. For example, in Figs. 4h,i, the secondary peak, which was the primary peak in Fig. 4g, becomes clearer. That is, the second most powerful peak is now consistent with the aerosol peak at the previous gate. In the lower gate, the aerosol peak cannot be identified in the original spectral output, while clipping makes this aerosol peak more prominent.

Although clipping reduces the intensity of the ground peak, there still remains the issue of identifying the aerosol peak in the presence of a more powerful ground peak. The method described in the next section addresses this issue.

b. Threading

We define threading as a method to identify and follow an aerosol peak in a weak signal regime and, in this case, the presence of stronger ground peak. There are several steps in the threading routine. First, the raw data are processed using an FFT, and then the ground is determined in the backscattered signal by identifying the gate with the strongest SNR. Identifying the ground return is essential because the ground is used as a reference point in the next step in which the chirp signature is detected. The linear pattern of the chirp signature near the ground helps to identify the height at which the ground signal first becomes powerful enough to interfere with the aerosol signal. Identification of this chirp signature in the profile is accomplished by starting at the ground (0 m s^{-1}) and following the linear trend up to the height where the radial velocity approaches ~ -2 m s^{-1} [first evidence of chirp (FEC) signature]. This height is the location where the ground return becomes more powerful than the aerosol return. In the next step of the threading routine, the radial velocity in the range gate above the FEC is determined and used as a starting point for the next threading step. In this step, radial velocities associated with the primary and secondary frequency peaks at the FEC are determined. All radial velocities at the FEC that do not fall within a predefined deviation from the radial velocity aloft are removed from further analysis. We tested this procedure with deviations from 1 to 5 m s^{-1} to determine what deviation would maximize the possibility of selecting radial velocities associated with the aerosol return. For a maximum radial velocity deviation of 5 m s^{-1}, we noticed that peaks associated with noise were occasionally selected. On the other hand, a maximum deviation of 1 m s^{-1} eliminated radial velocities that were related to the aerosol return and, in our example, were a result of a low-level wind maximum (see section 5). As a compromise, only radial velocities that deviate less than 2 m s^{-1} of the radial velocity aloft are retained. It is important to note that radial velocities at a nadir angle of 20° equate to ~1/3 of the horizontal wind motion. Therefore, a radial velocity of 2 m s^{-1} is equivalent to ~6 m s^{-1} in the horizontal. As an additional constraint, we also eliminated radial velocities that fall within ±2 m s^{-1} of the radial velocity associated with the ground return. This additional constraint reduces the likelihood of incorrectly assigning a radial velocity created by the ground return. This procedure is repeated for the next range gate closer to the ground using the newly determined radial velocity at the range gate above.

c. Combining clipping and threading

The impact of clipping and threading on the radial velocity profiles is shown in Fig. 5, which is based on the spectral output in Figs. 2 and 4 (third column). In Fig. 5, radial velocities associated with the primary and secondary frequency peaks are shown. The horizontal dotted line

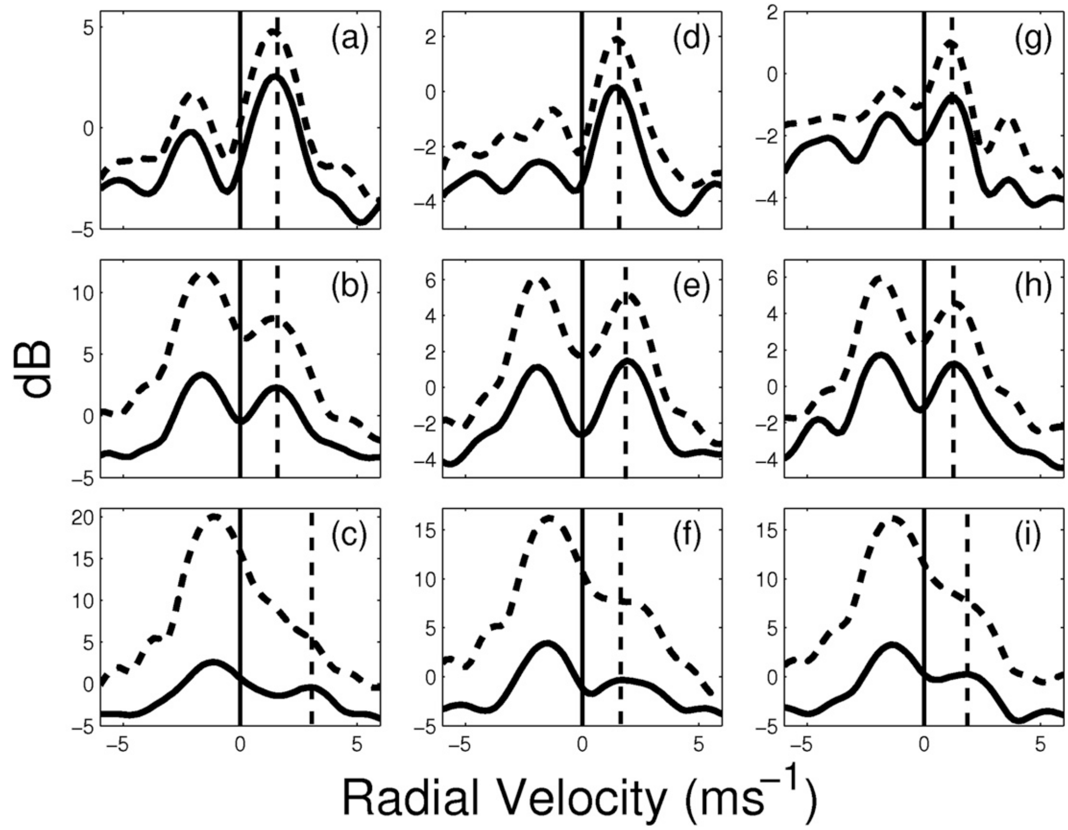

FIG. 4. As in Fig. 2, but for both original (dashed) and clipped (solid) data. (c),(f),(i) The location of the aerosol peak (vertical dashed line) is denoted, which can now be identified in the lowest range gate after clipping. Zero velocity as determined by transmitted/monitor pulse (vertical solid line) is also shown.

represents the height where the FEC was identified in the threading routine. At that height the ground peak is larger than the aerosol peak. The chirp signature can readily be observed in the original radial velocity profile where the radial velocities change linearly from -2 m s^{-1} at 150 m AGL to 0 m s^{-1} at the ground. Using the threading routine, we gain an additional radial velocity range gate below the height where the chirp signature was identified (arrow in Fig. 5a). In Fig. 5b, the radial velocities associated with the primary and secondary frequency peaks are shown after the clipping routine is applied. Note that clipping does not remove the spectral peak associated with the ground return. However, the secondary aerosol peaks in the region influenced by the ground can now be resolved at the 100-m range gate (arrow in Fig. 5b), resulting in two additional radial velocities when the threading routine is applied (two arrows in Fig. 5c).

We applied clipping and threading to all data collected on the flight on 12 November 2007 (3412 radial velocity profiles in 285 conical scans), resulting in an additional 50-m range gate in 47% of all the radial velocity profiles compared to 38% with threading only (Table 2). Two or more additional 50-m range gates were obtained in 23% of the radial velocity profiles, compared to 13% with threading only. Recall that the “true” radial velocities cannot fall within ± 2 m s^{-1} of the linear radial velocity profile (the chirp signature) induced by the ground interference. This constraint by itself removes about 50% of the radial velocities from being considered in the final steps of the routine.

5. Impact of two-step approach on vertical wind profiles

Next, we investigate the impact of the two-step approach on wind speed and direction profiles. First, radial velocities are determined using the approach described in section 4. Then, wind speed and direction are determined from these radial velocities using the VAD technique (see section 2). Some radial velocities in the VAD processing may represent the true aerosol radial velocity while others may represent the radial velocity induced by ground interference. To further minimize the risk that the additional wind speed and direction

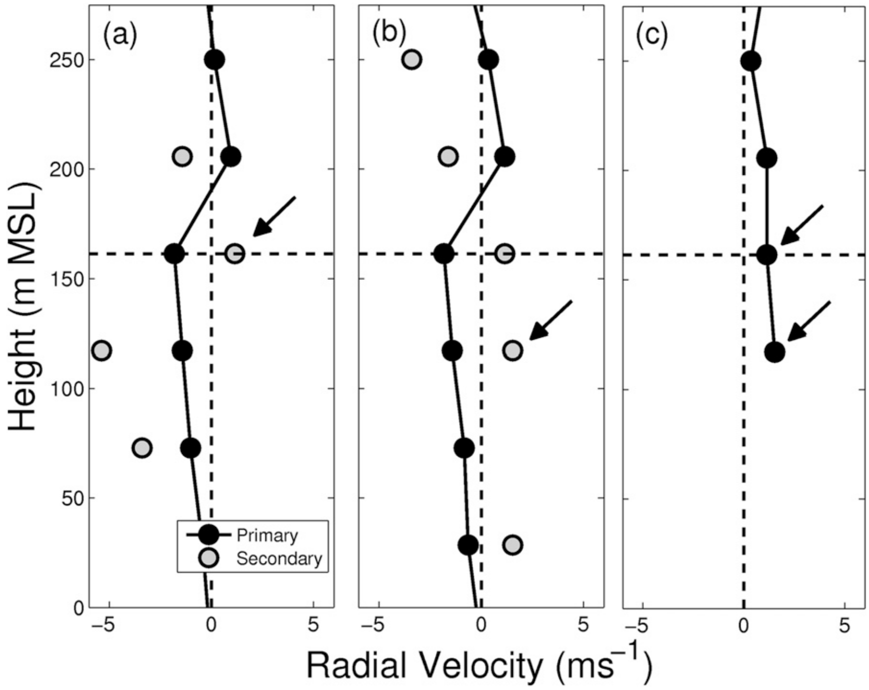

FIG. 5. Vertical profiles of radial velocities (filled circles connected by a solid line) are shown (a) before and (b) after clipping and (c) after clipping and threading. Primary (filled black circles) and secondary peaks (filled gray circles) are shown in (a) and (b). Note that the radial velocities associated with the primary peak do not change as a result of clipping. The level of the FEC (dashed horizontal line) is denoted. The secondary peak at this height is the aerosol peak, which is correctly assigned the radial velocity after threading [indicated by an arrow in (a) and (c)]. Similarly, at the range gate below the FEC level, the secondary peak after clipping is the aerosol peak, which is correctly assigned the radial velocity after threading [indicated by an arrow in (b) and (c)]. In this example, clipping and threading results are applied in reliable wind information for two additional range gates (or 100 m) closer to the surface.

values are affected by ground interference, we require that these values can only deviate a certain amount from the values obtained above the first range gate with ground interference, similar to our approach with the radial velocities. In our example, we require the change in wind speed and direction between these consecutive range gates is less than 5 m s^{-1} and 90°, respectively. While it is physically possible to have a larger shift in wind speed and direction over a 50-m height interval, the likelihood of this occurring is small below the nominal top of the daytime mixed layer (>300 m). During the nighttime, when there can be decoupling between the shallow nocturnal boundary layer and the free tropospheric layer above, this constraint on shear would have to be altered. We furthermore require that the RMSE of the sine fit is less than 0.5 m s^{-1}. This procedure is repeated with the next range gate closer to the surface until the wind speed and direction deviations or the sine fit RMSE exceed the threshold values.

We demonstrate the changes in near-surface wind retrieval using the above approach with an example where we compare the lidar-derived wind profiles with winds obtained from a 915-MHz radar wind profiler (Fig. 6). This wind profiler is located at the Fort Ord Army Post and operated by the Naval Postgraduate School in Monterey, California. The wind profiler measures winds at 50-m resolution in a short-range high-resolution mode from a height of 112 to 1000 m AGL. The 30-min-averaged profiles from this high-resolution mode are compared to the lidar-derived winds. The lidar wind profile is located 8.5 km up the valley from the wind profiler. In this particular case, the effect of

TABLE 2. Percentage of radial velocity profiles in which one or more additional range gates were identified using threading only and using a combination of clipping and threading.

	Threading	Clipping and threading
One additional gate	38%	47%
Two additional gates	13%	23%
Three additional gates	5%	9%

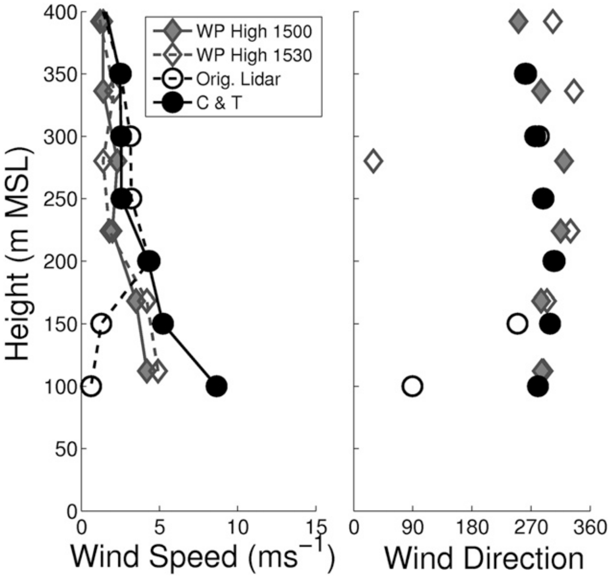

FIG. 6. Wind speed and wind direction derived from airborne Doppler lidar before and after clipping and threading (open and filled circles, respectively), and microwave wind profiler (WP) acquired at 1500 (filled triangle) and 1530 LST (open triangle). Lidar profile was acquired at 1512 LST and separated 8.5 km from wind profiler.

the ground on the wind speeds is obvious for range gates below 200 m MSL (Fig. 6). The original lidar wind speeds decrease sharply at these range gates, which is opposite of the trend in the wind profiler data. Using the procedure described above, the retrieved airborne Doppler-derived winds compare well with those of the wind profiler. Perfect agreement between wind profiler and lidar-derived winds is not expected given the distance between the two sampling volumes and the differences in sampling and averaging time. It is clear though, that the wind speed and direction from improved airborne DWL wind retrievals and the microwave wind profiler show a similar structure.

Another example of the changes in retrieved winds resulting from the two-step approach is shown in Figs. 7 and 8 . These two figures show along-valley flows for five flight legs at four range gates (from 350 to 200 m MSL in 50-m intervals) using the original and improved wind retrieval procedure, respectively. This example demonstrates how the improved procedure results in the identification of an along-valley wind acceleration close to the surface and an associated wind maximum near the surface. This is particularly apparent at 200 m (Figs. 7d and 8d) where the winds from the original signal processing routines are all predominantly below 2 m s^{-1}. The along-valley acceleration was also evident in available data from a surface meteorological network along the Salinas Valley (DEW).

The additional range gates provide us with important information on wind structure near the surface. We found that with our two-step approach, wind profiles were extended downward for at least 50 m in 34% of the profiles and 100 m or more in 14% of the profiles obtained during the flight on 12 November 2007.

6. Discussion

The examples presented above illustrate how we can improve near-surface wind retrieval in the presence of strong ground returns using some simple but robust methods. Inherent to the current implementation of our two-step approach is a considerable degree of subjectivity, such as the determination of the threshold intensity in clipping. The threshold intensity is affected by the SNR such that for a given threshold intensity, a large increase in SNR near the surface (e.g., because of fog or smoke) could reduce the information content of the aerosol signal relative to the ground signal. That is, some of the desired aerosol signal could be clipped as well. Also, the tracking of aerosol peaks in the vertical only works well if the aerosol radial velocity is sufficiently separated from ground interference–induced velocity (i.e., the chirp signature). In our current implementation of the two-step approach, we do not track aerosol radial velocities to the surface if the absolute difference with the radial velocity associated with the chirp signature is smaller than 2 m s^{-1}. Otherwise, the likelihood of selecting a radial velocity affected by ground interference is large.

While our approach reduces ground interference in the raw signal domain, another approach could be to improve the identification of the aerosol peak in the spectral domain. We briefly discuss and illustrate two possibilities. One possibility is to implement a band-stop filter (e.g., Smith 1997). The band-stop filter targets a range of the frequency spectrum containing the frequencies associated with the chirp signature in this case, and removes the contribution from these frequencies. A second possibility is to apply the derivative method that uses the second derivative of the original spectrum to enhance the resolution of peaks in a spectrum (Butler and Hopkins 1970).

We illustrate these methods and compare them with clipping in Fig. 9 using simulated time series of return signals. The simulated data consist of multiple sinusoidal signals: 1) a ground return signal at -1 m s^{-1} with a maximum intensity of 8 dB, 2) an aerosol signal at -0.5 m s^{-1} with an intensity of 4 dB, and 3) three randomized noise signals with varying intensities between 1 and 2 mV. The detectable contribution of the ground return begins just prior to 1 μs and increases to the

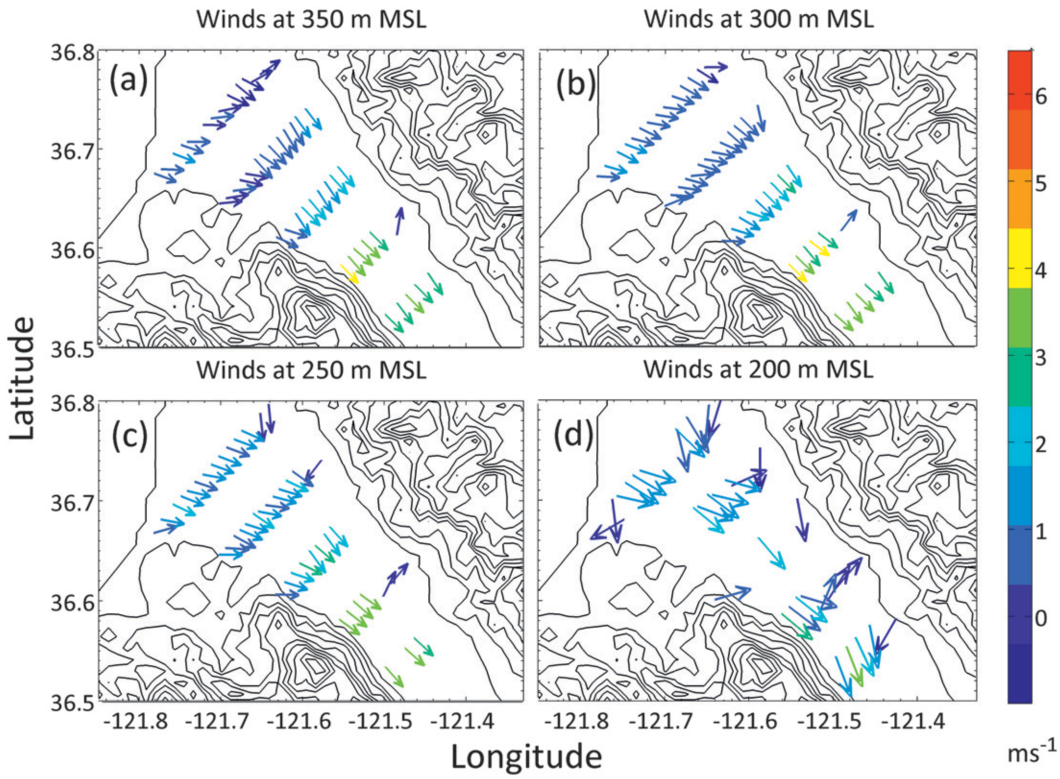

FIG. 7. Horizontal winds in the Salinas Valley at (a) 350, (b) 300, (c) 250, and (d) 200 m MSL determined using the original signal processing procedure.

maximum intensity of 8 dB or larger. These higher values are due to the addition of the above-mentioned signals. To simulate the signal from the TODWL system the sampling frequency is set to 100 MHz.

In the first example, the original raw data time series and its corresponding periodogram are shown in Figs. 9a,b, respectively. The vertical dashed line represents the frequency (or radial velocity) where the aerosol peak should occur (-0.5 m s^{-1}). In the original periodogram (Fig. 9b), the only discernible peak above the noise level is due to the ground return. The aerosol peak can only be observed as a small ''bump'' on the side of the larger ground peak.

In the second example, the raw data that exceed 7 dB from the mean are clipped. A value of 7 dB is chosen because the aerosol signal falls below and the ground signal exceeds this value. The resulting periodogram (Fig. 9c) has an easily identifiable aerosol peak with a secondary peak resulting from the ground return.

In the third example, a band-stop filter is applied to the original raw signal data. The filter is Gaussian shaped with the center at -1 m s^{-1} and a maximum width of 0.75 m s^{-1}. The resulting periodogram (Fig. 9d) has an identifiable aerosol peak while the ground peak is significantly reduced. This method works well in this case because we knew exactly where to expect the ground peak. In practice, however, the height above the ground of the chirp-induced frequency sweep in the ground reflectance is highly variable and unknown a priori. This makes the implementation of this method difficult for real data. Clipping, on the other hand, does not require prior knowledge of the chirp-induced frequency sweep.

In the fourth example, the aerosol peak is enhanced with the derivative method. With this method the weighted second derivative of the original spectrum is subtracted from the original spectrum. The weighting factor is user defined and depends on the allowance for accurate signal strength versus resolution enhancement. In this particular instance, we use a weighting factor of 3. The derivative method results in an enhanced aerosol peak, but we also notice that the radial velocity has shifted by 0.1 to -0.6 m s^{-1} (Fig. 9e). This shift is due to the overlapping frequency bins and is dependent on the weighting factor. For an implementation with real data, these shifts must be accounted for and corrected on a case-by-case basis.

From the above examples, it is clear that there are alternatives to clipping in the two-step approach, but these may be more difficult to implement in the processing of real data. While we continue to explore these alternative

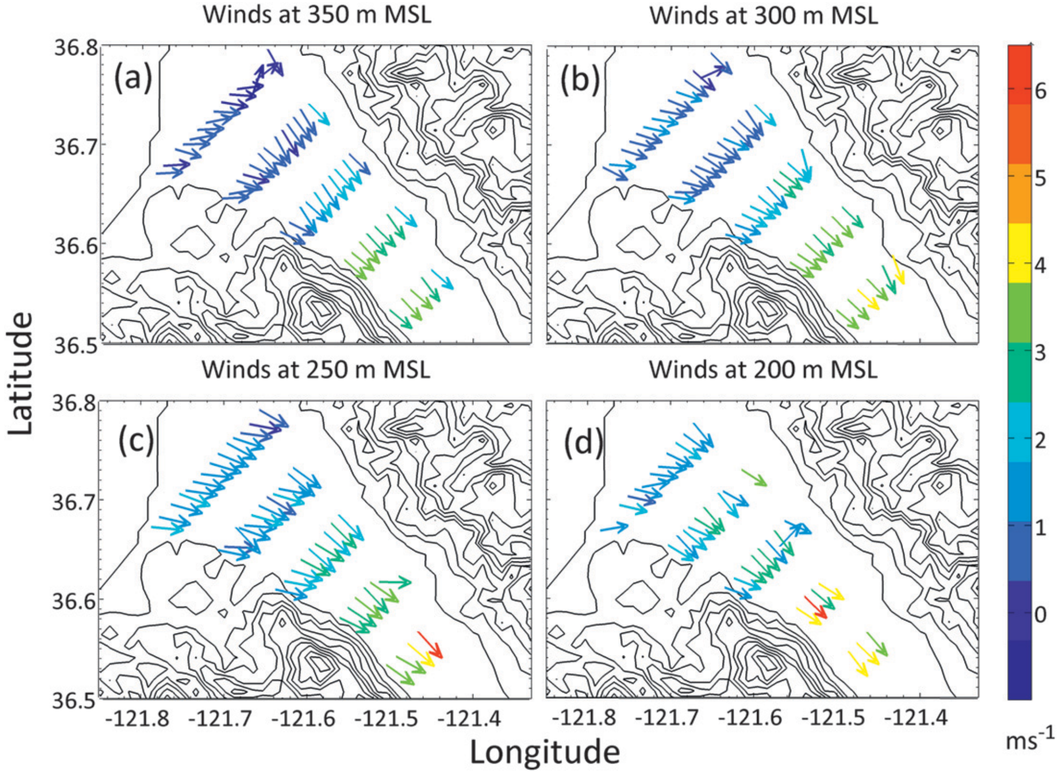

FIG. 8. As in Fig. 7, but for horizontal winds determined after applying clipping and threading.

methods, the robustness and easiness of clipping make this method preferable in our current data-processing routines.

7. Summary

The retrieval of winds from airborne Doppler lidar within the lowest range gates above the surface is confounded by the signal from the ground return, which interferes with the aerosol signal. We demonstrated the effect of ground interference using simulated and realistic examples and introduced a two-step approach to address this challenge. The approach includes 1) the reduction of ground return signal in the raw backscatter data (clipping) and 2) the identification and tracking of a spectral peak associated with the aerosol signal down to the surface (threading).

We showed that the wind retrieval is improved with this approach using data obtained over the Salinas Valley in California. The approach typically results in the retrieval of winds in one or two additional range gates (in our case, 50–100 m) closer to the surface. These winds compare well with independent measurements from a neighboring microwave wind profiler. The additional range gates reveal a significant low-level region of increased wind speed that was not identified previously but is consistent with data from a surface network of anemometers (DEW).

The approach used here serves as a first step to improving the near-surface wind retrieval from airborne Doppler lidar. While the current approach appears robust, we explained some limitations and provided examples of alternative approaches. In particular, we discussed approaches that focus on the identification of aerosol peaks in the spectral domain rather than on reducing the intensity of the ground return in the raw data. Examples include the band-stop filter, which removes the ground peak and the derivative method and enhances the aerosol peak. Examples of these approaches were shown using simulated data. The implementation of these approaches is more difficult for real data and would need further research.

Clearly, improving the near-surface wind retrieval enhances the potential of airborne Doppler lidar for atmospheric boundary layer research. This technique will be equally important for space-based lidars that may have longer pulse lengths. In this case an additional range gate could mean the difference between a measurement within and outside the atmospheric boundary layer.

This paper only highlighted one challenge with airborne Doppler data that we have focused on in our recent research activities. While airborne Doppler lidar

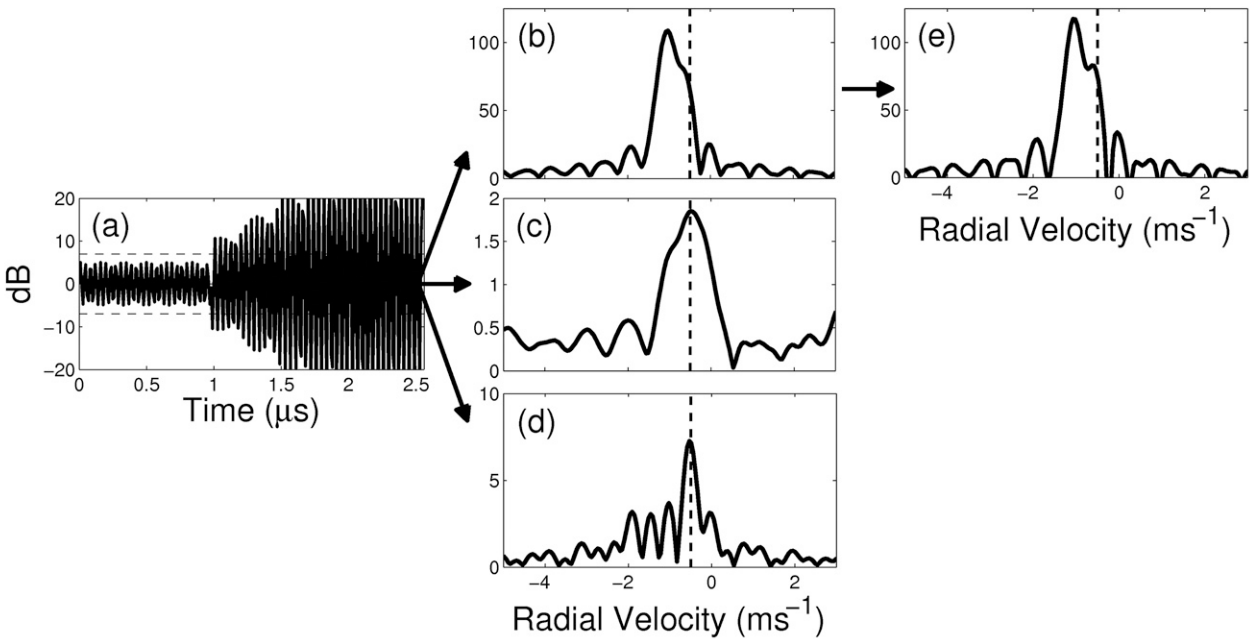

FIG. 9. (a) Simulated raw data that resembles a mixture of a ground return and an aerosol return. (b) An FFT of the raw data produces a periodogram consisting of a strong ground peak at -1 m s^{-1} and a weak aerosol peak at -0.5 m s^{-1} (dashed line). Periodogram (c) after raw data are clipped, (d) after raw data are band-stop filtered, and (e) resolution enhanced.

can already provide us with detailed documentation and improved understanding of atmospheric dynamics, addressing these and other challenges is important in the further development of airborne and spaceborne Doppler lidars.

Acknowledgments. This research was supported by Grant W911NF-09-1-0076 from the Army Research Office and Contract N00014-11-1-0450 from the Office of Naval Research. The Twin Otter Doppler Wind Lidar flights were funded by Dr. Steven Mango, chief scientist for the Integrated Program Office of the National Polar Orbiting Environmental Satellite System. Dr. Robert Bluth, director of the Center for Interdisciplinary Remotely Piloted Aircraft Studies provided significant institutional support for the wind lidar missions.

REFERENCES

Baker, W. E., and Coauthors, 1995: Lidar-measured winds from space: An essential component for weather and climate prediction. *Bull. Amer. Meteor. Soc.,* **76,** 869–888.

Banta, R. M., L. D. Olivier, and D. H. Levinson, 1993: Evolution of the Monterey Bay sea-breeze layer as observed by pulsed Doppler lidar. *J. Atmos. Sci.,* **50,** 3959–3982.

——, L. S. Darby, J. D. Fast, J. O. Pinto, C. D. Whiteman, W. J. Shaw, and B. W. Orr, 2004: Nocturnal low-level jet in a mountain basin complex. Part I: Evolution and effects on local flows. *J. Appl. Meteor.,* **43,** 1348–1365.

Bastin, S., P. Drobinski, A. M. Dabas, P. Delville, O. Reitebuch, and C. Werner, 2005: Impact of the Rhone and Durance valleys on sea-breeze circulation in the Marseille area. *Atmos. Res.,* **74,** 303–328.

——, and Coauthors, 2006: On the interaction between sea breeze and summer mistral at the exit of the Rhône Valley. *Mon. Wea. Rev.,* **134,** 1647–1668.

Browning, K., and R. Wexler, 1968: The determination of kinematic properties of a wind field using Doppler radar. *J. Appl. Meteor.,* **7,** 105–113.

Butler, W. L., and D. W. Hopkins, 1970: An analysis of fourth derivative spectra. *Photochem. Photobiol.,* **12,** 451–456.

De Wekker, S. F. J., K. S. Godwin, G. D. Emmitt, and S. Greco, 2012: Airborne Doppler lidar measurements of valley flows in complex coastal terrain. *J. Appl. Meteor. Climatol.,* in press.

Drobinski, P., C. Heaberli, E. Richard, M. Lothon, A. M. Dabas, P. H. Flamant, M. Furger, and R. Steinacker, 2003: Scale interaction processes during the MAP IOP-12 south Foehn event in the Rhine Valley. *Quart. J. Roy. Meteor. Soc.,* **129,** 729–753.

Emmitt, G. D., C. O'Handley, S. A. Wood, R. Bluth, and H. Jonsson, 2005: TODWL: An airborne Doppler wind lidar for atmospheric research. Preprints, *Second Symp. on Lidar Atmospheric Applications*, San Diego, CA, Amer. Meteor. Soc., P2.3. [Available online at http://ams.confex.com/ams/pdfpapers/85828.pdf.]

Lhermitte, R. M., and D. Atlas, 1961: Precipitation motion by pulse Doppler radar. *Proc. Ninth Weather Radar Conf.*, Kansas City, MO, Amer. Meteor. Soc., 218–223.

Menzies, R. T., 1986: Doppler lidar atmospheric wind sensors: A comparative performance evaluation for global measurement applications from earth orbit. *Appl. Opt.,* **25,** 2546–2553.

Post, M. J., and W. D. Neff, 1986: Doppler lidar measurements of winds in a narrow mountain valley. *Bull. Amer. Meteor. Soc.,* **67,** 274–281.

Pu, Z., L. Zhang, and G. D. Emmitt, 2010: Impact of airborne Doppler wind lidar data on numerical simulation of a tropical cyclone. *Geophys. Res. Lett.,* **37,** L05801, doi:10.1029/2009GL041765.

Rahm, S., 1995: Measurement of a wind field with an airborne continuous-wave Doppler lidar. *Opt. Lett.,* **20,** 216–218.

Reitebuch, O., H. Volkert, C. Werner, A. Dabas, P. Delville, P. Drobinski, P. H. Flamant, and E. Richard, 2003: Determination of flow across the Alpine ridge by a combination of airborne Doppler lidar, routine radio-soundings and numerical simulations. *Quart. J. Roy. Meteor. Soc.,* **129,** 715–727.

Rucker, M., R. M. Banta, and D. G. Steyn, 2008: Along-valley structure of daytime thermally driven flows in the Wipp Valley. *J. Appl. Meteor. Climatol.,* **47,** 733–751.

Rye, B. J., and R. M. Hardesty, 1993a: Discrete spectral peak estimation in incoherent backscatter heterodyne lidar. I. Spectral accumulation and the Cramer-Rao lower bound. *IEEE Trans. Geosci. Remote Sens.,* **31,** 16–27.

——, and ——, 1993b: Discrete spectral peak estimation in incoherent backscatter heterodyne lidar. II. Correlogram accumulation. *IEEE Trans. Geosci. Remote Sens.,* **31,** 28–35.

Smalikho, I. N., 2003: Techniques of wind vector estimation from data measured with a scanning coherent Doppler lidar. *J. Atmos. Oceanic Technol.,* **20,** 276–291.

Smith, S. W., 1997: *The Scientist and Engineer's Guide to Digital Signal Processing.* California Technical Publishing, 626 pp.

Van Vleck, J., and D. Middleton, 1966: The spectrum of clipped noise. *Proc. IEEE,* **54,** 2–19.

Weissmann, M. D., and C. Cardinali, 2007: Impact of airborne Doppler lidar observations on ECMWF forecasts. *Quart. J. Roy. Meteor. Soc.,* **133,** 107–116.

——, F. J. Braun, L. Gantner, G. J. Mayr, S. Rahm, and O. Reitebuch, 2005: The alpine mountain–plain circulation: Airborne Doppler lidar measurements and numerical simulations. *Mon. Wea. Rev.,* **133,** 3095–3109.

Werner, C., 2005: Doppler wind lidar. *Lidar: Range-Resolved Optical Remote Sensing of the Atmosphere*, C. Weitkamp, Ed., Series in Optical Sciences, Vol. 102, Springer, 339–342.